Pacific Northwest
NATIONAL LABORATORY

PNNL-35097

Enhanced Tritium Retention in LiAlO2 Pellets via Engineered Glazes

Tritium Science Project

September 2023

John Hardy
Michael Powell
Matt Chou
Larry Bagaasen

U.S. DEPARTMENT OF ENERGY

Prepared for the U.S. Department of Energy
under Contract DE-AC05-76RL01830

DISCLAIMER

PACIFIC NORTHWEST NATIONAL LABORATORY
operated by
BATTELLE
for the
UNITED STATES DEPARTMENT OF ENERGY
under Contract DE-AC05-76RL01830

Printed in the United States of America

Available to DOE and DOE contractors from
the Office of Scientific and Technical Information,
P.O. Box 62, Oak Ridge, TN 37831-0062
www.osti.gov
ph: (865) 576-8401
fox: (865) 576-5728
email: reports@osti.gov

Available to the public from the National Technical Information Service
5301 Shawnee Rd., Alexandria, VA 22312
ph: (800) 553-NTIS (6847)
or (703) 605-6000
email: info@ntis.gov
Online ordering: http://www.ntis.gov

PNNL-35097

Enhanced Tritium Retention in LiAlO2 Pellets via Engineered Glazes

Tritium Science Project

September 2023

John Hardy
Michael Powell
Matt Chou
Larry Bagaasen

Prepared for
the U.S. Department of Energy
under Contract DE-AC05-76RL01830

Pacific Northwest National Laboratory
Richland, Washington 99354

Abstract

This project investigated the impact of adding a thin (10 – 50 μm) layer of amorphous glaze to the surface of a TPBAR pellet on its retention of helium, hydrogen (as a surrogate for tritium), and water (as a surrogate for tritiated water). The hypothesis was that the glaze would significantly reduce permeation of hydrogen species with a lesser impact on hindering helium permeation. A non-crystallizing soda-lime-silicate glass, known as SCN-1, was selected for this proof-of-concept study. It was found that continuous glaze layers of the desired thickness could be applied to the pellets with two or more dip coats, depending on the targeted thickness. At 330°C, the glaze was found to have a permeability that was lower than that of the pellet by a factor of ~10^6, implying that a thin 10 – 50 μm layer can significantly increase pellet retention of hydrogen. Meanwhile, the permeation rate of helium through the glaze was found to be ~20 times higher than that of hydrogen or water. An unanticipated outcome of the study was that unglazed pellets were measured to have hydrogen diffusivities that are a factor of ~10^5 greater than the diffusivity value used in the TPBAR COMSOL model to achieve observed tritium retention rates. When the higher measured diffusivity was substituted into the model and the model was run with all tritium species in the pellet in the form of T_2O at a partial pressure of 20 Pa in equilibrium with LiOT, the resulting retention was 50% after 500 days.

Acronyms and Abbreviations

CTE – Coefficient of Thermal Expansion
EDS – Energy Dispersive Microscopy
HT – High Temperature
OD – Outer Diameter
OM – Optical Microscopy
RGA – Residual Gas Analyzer
RT – Room Temperature
SEM – Scanning Electron Microscopy
T_g – Glass Transition Temperature
TMIST – TPBAR Materials Irradiation Separate-effects Test
TPBAR – Tritium Producing Burnable Absorber Rods

Contents

Figures

Tables

1.0 Introduction

Past TMIST and Tritium Science efforts have shown that tritium mobility in pellets is greatly enhanced by the presence of pellet porosity (either present in the as-fabricated pellet or because of irradiation induced microstructural changes), grain boundaries, and near-neighbor Li vacancies. This work investigated using a stable amorphous glaze on exterior pellet surfaces to act as a non-porous, grain boundary-free, lithium-free barrier to the migration of tritium gas and tritiated water out of the pellet. The hypothesis was that this barrier might significantly increase pellet tritium retention while consuming only small portions of TPBAR void volume. Additionally, the glaze material was selected to preferentially allow He gas to more readily escape the glazed pellets than the tritium species, therefore minimizing additional He contribution to interior pellet pressure. Helium readily permeates through some glasses while hydrogen and tritium permeate at rates less than 1/10th that of helium (Leiby and Chen, 1960). Water molecules usually permeate at even lower rates (Wakabayashi and Tomozawa, 1989). This project experimentally investigated whether a glaze layer applied to the pellet surface allowed selective helium release while promoting tritium retention by a combination of physical restriction and the effects of $T_2O/LiAlO_2$ equilibrium. For example, in addition to being a barrier to tritium gas permeation, the glaze may stabilize hydroxide-type phases under reactor conditions, thereby retaining large quantities of tritium in a solid form in the pellet. If LiOT formation occurred according to the following reaction, Figure 1 shows that only a modest backpressure of T_2O (~ 20 Pa or 2x10-4 atm) is required to maintain the solid/gas equilibrium (Katayama, et al. 2016).

$$5LiAlO_2 + 2n \rightarrow LiAl_5O_8 + 2LiOT + 2He$$

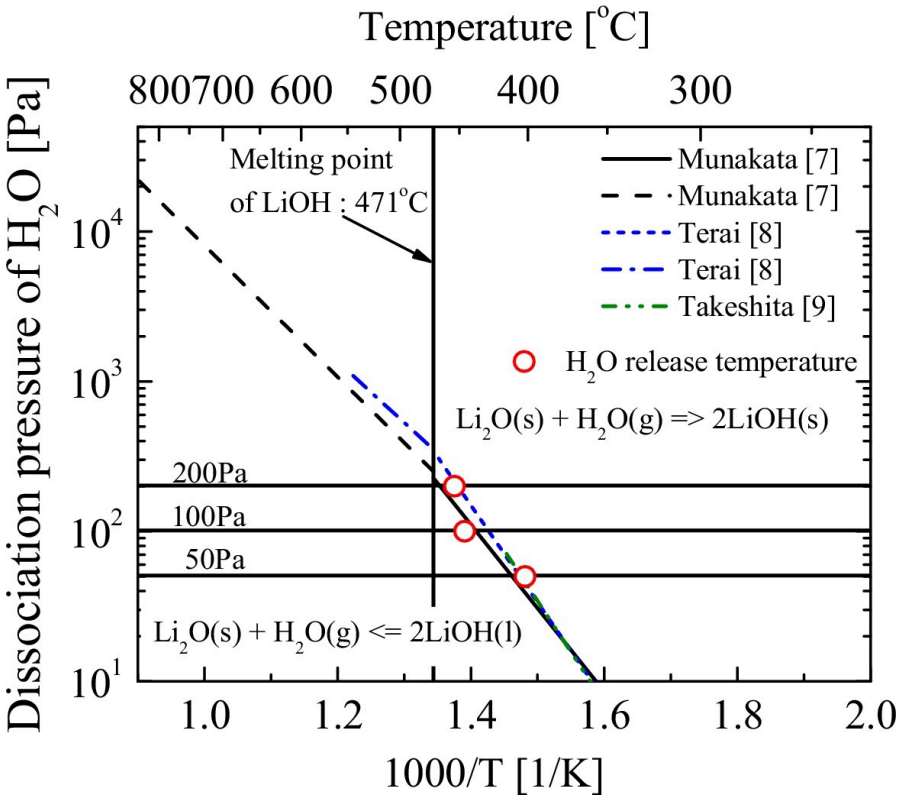

Figure 1.1. Equilibrium vapor pressure of water over LiOH as a function of temperature.

2.0 Experimental

2.1 Glaze Characterization, Dip-Coating, and Test Pellet Preparation

A soda-lime silicate glass (SCN-1) was selected for this project as the candidate glazing material, due to its wettability, vitreous nature (no grain boundaries), and good match in CTE with lithium aluminate as compared to traditional glaze materials (web ref). The silicate glass also has a permeation coefficient of interest among various glasses (Norton 1953). This glass has been used as a compliant sealing glass for solid oxide fuel cells where it remains vitreous after high temperature firing and long-term operation (Chou et al 2012). It has a reasonably high coefficient of thermal expansion (CTE) of ~10-11x10^{-6}/ºC (Liu et al 2010), very low glass transition temperature of ~500ºC, and good compatibility with $LiAlO_2$ material. The chemical composition of SCN-1 glass (SEM-COM, Toledo, OH) is listed in Table 2.1.

Table 2.1. Chemical composition of glass SCN-1

oxide	Al2O3	BaO	CaO	Fe2O3	K2O	MgO	Na2O	TiO2	ZnO	ZrO2	Li2O	B2O3	SiO2
mole%	1.84	3.57	3.96	0.09	7.07	1.03	7.83	0.45	0.01	0.01	0.05	0.03	74.06

Dip-coating was used to coat the as-received dense $LiAlO_2$ pellets (2” long tube with OD ~1 mm). A slurry was prepared by mixing attrition-milled SCN-1 powders with an organic binder solution and isopropanol in a plastic bottle with zirconia milling media for 4 hours on a ball mill. A wetting and coating thickness study was performed on a thin (~0.5 mm) rectangular ceramic coupon (~1 cm x 2 cm) composed of dense zirconia layer to mimic the wetting behavior of glaze on typical oxides. The ceramic coupon was dip-coated in the mixed slurry by hand using tweezers. No controlled rate for removing coupons from slurry was pursued since the coupon is rather short. The as-coated coupons were then dried in an oven at ~100ºC for a few minutes between dip-coatings. In this work, we have dip-coated between one (1x) and four (4x) layers. After coating and drying, the coupons were fired to 450ºC for binder burn out, followed by 900ºC for 2h for wetting and glazing before cooling to room temperature. To characterize the wetting and morphology of glaze, optical microscopy (OM) was used. To measure the resulting glaze thickness, the coated rectangular sample was hand ground on sandpaper to smooth the edges. The glaze thickness was determined with OM in 10 locations and the average thickness was reported. The CTE of the as-received $LiAlO_2$ pellet was also characterized with a dilatometer.

Permeation test samples were prepared in two forms: short (2”) as-received pellets and long (6”) joined pellets. For the short pellet samples, the pellet needs to be plugged on one end before the permeation test can be conducted. A stainless steel (SS441) plug was machined and inserted into one open end of the pellet and a sealing glass (G18, CTE ~12.5x10^{-6}/ºC) was used due to its excellent CTE matching with $LiAlO_2$ (CTE ~12.5x10^{-6}/ºC), good wettability, and sufficient strength after firing. Later in the project, it was found that longer pellet samples would be more suitable for permeation tests, allowing the test time to be reduced and decreasing the background noise in the results. To make long pellet samples, three 2” pellets are first joined end-to-end with G18 glass and fired to 900ºC. The long sample was then plugged at one open end with a composite of G18 and granules of $LiAlO_2$. The granules of $LiAlO_2$ were prepared crushing the as-received pellets with a pestle and mortar. A typical example of a glazed short pellet sample and an unglazed long one is shown in Fig. 2.1 left and right, respectively.

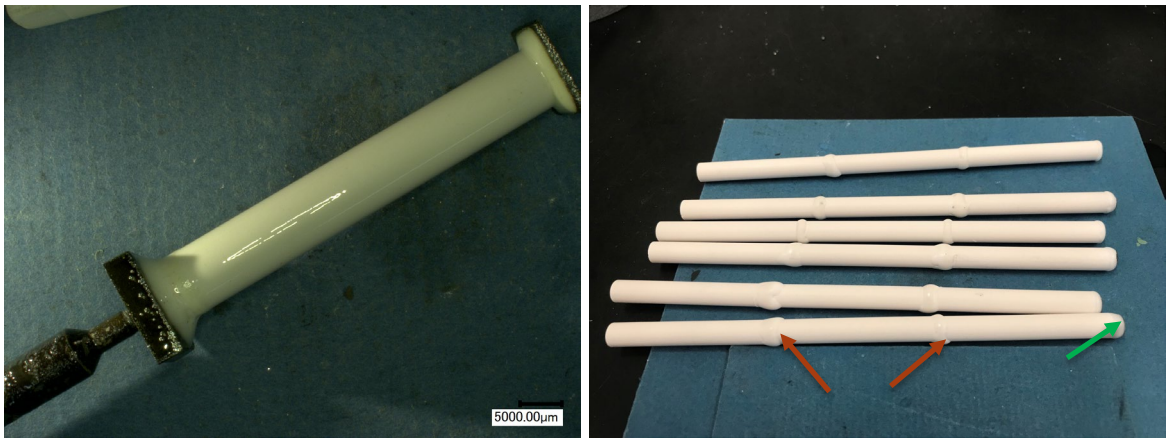

Figure 2.1. (Left) glazed short pellet sample with end cap sealed, and (Right) unglazed long joined (red arrow) pellet sample with one end plugged (green arrow).

2.2 Permeation Measurement Apparatus Description

Measurement of the gas permeability of the glazed $LiAlO_2$ pellets required development of an appropriate test fixture. Initially, attempts were made to bond the $LiAlO_2$ pellets to dense alumina tubing, but the thermal expansion mismatch between the two ceramics resulted in poor bonding.

The thermal expansion behavior of the pellets is well-matched by 441 stainless steel, so for each sample, a small plate of SS441 was welded to a 6-inch length of 316SS tubing. This plate/tube was then bonded to one end of a $LiAlO_2$ pellet with a glass seal. The other end of the pellet was capped using a glass seal to bond another SS441 plate to the pellet. This arrangement is shown in Figure 2.2 below.

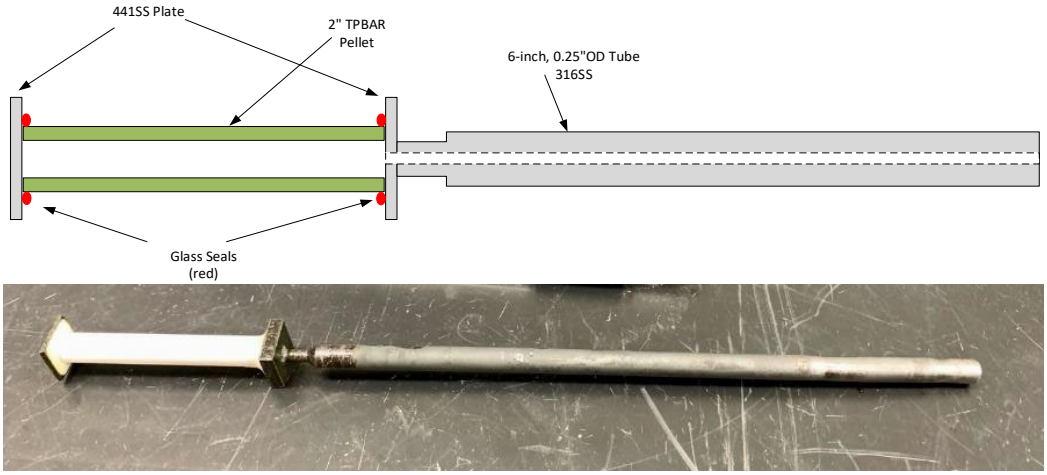

Figure 2.2. Test fixture for pellet permeation measurements

Multiple $LiAlO_2$ pellets were bonded to the test fixtures with the SS441 plates. Each pellet was then tested to determine its helium and hydrogen permeation rates before glaze was applied. The permeation tests involved loading each test fixture into a 1-liter pressure vessel and evacuating the vessel to less than 0.1 Torr. The vessel was then backfilled with helium or hydrogen and the rate of permeation through the pellet measured using a He/H_2 leak detector connected to the open end of the 316SS tube. A schematic of the test apparatus is provided in Figure 2.3 below.

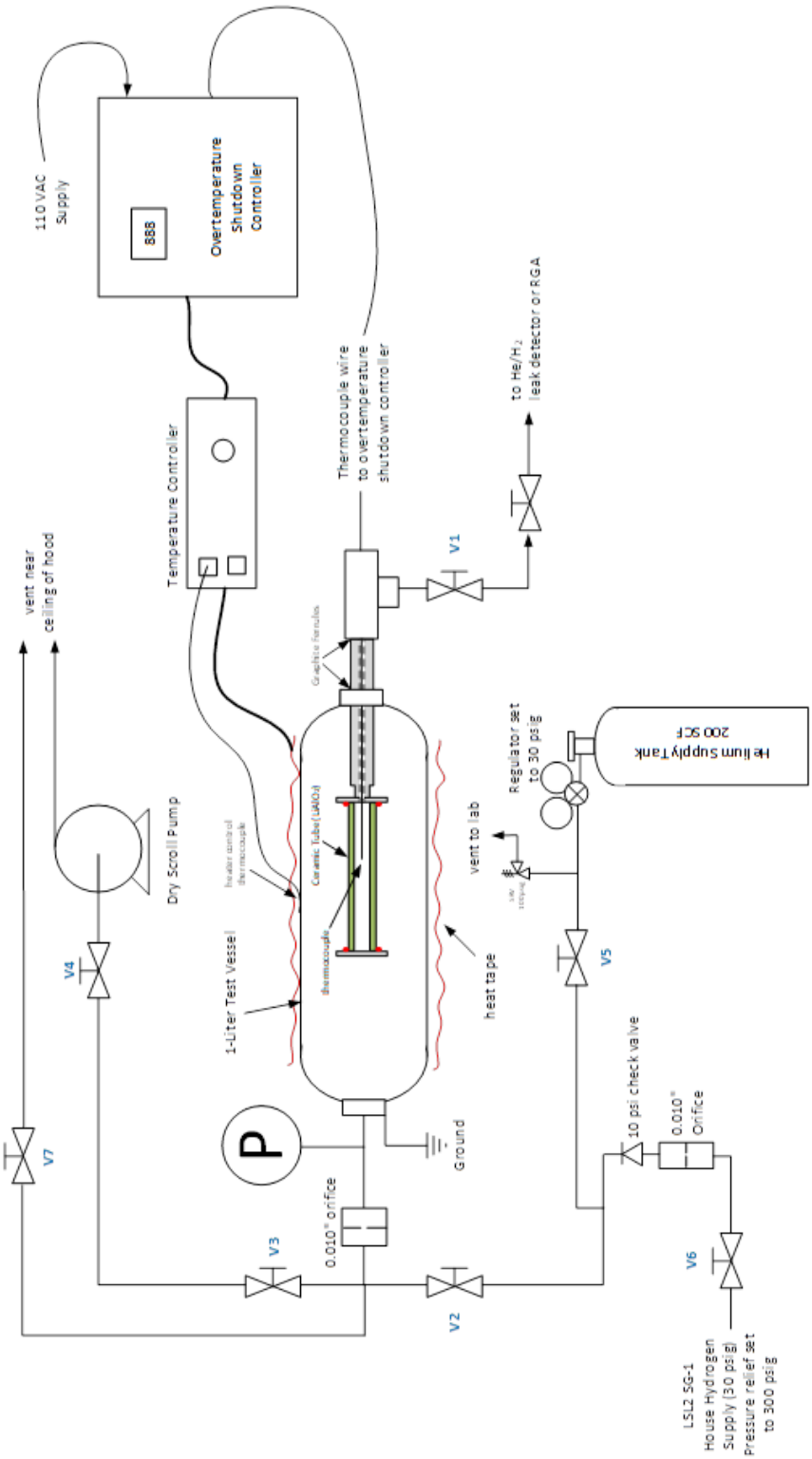

Figure 2.3. Schematic of pellet gas permeation test apparatus

In most cases, the helium or hydrogen gas was supplied at a pressure of 1 atm (absolute) and the resulting helium/hydrogen leak rates quantified by the Pfeiffer ASM340 leak detector. A photograph of the apparatus with the leak detector is provided in Figure 2.4 below. The gas permeation rates for the unglazed samples were measured to allow adjustment of the glazed-sample data as necessary to account for the permeation restriction of the pellet versus that of the glaze layer.

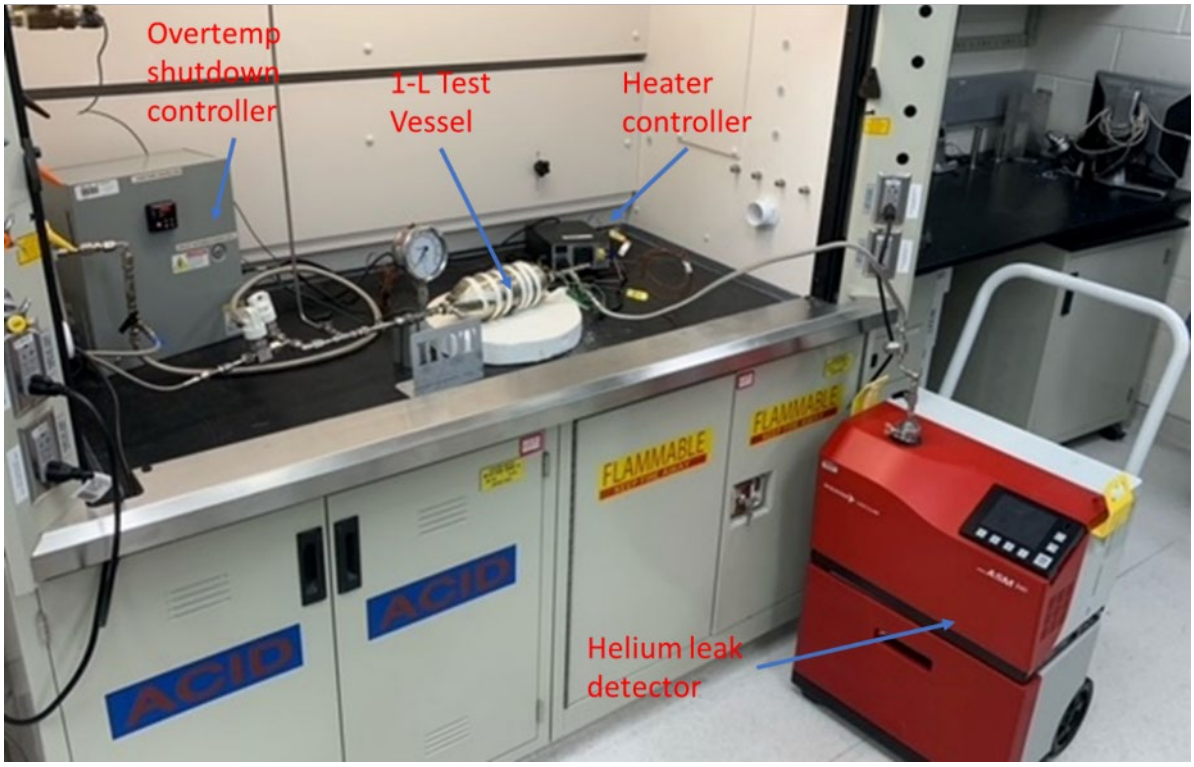

Figure 2.4. Pellet gas permeation rate apparatus with He/H_2 leak detector

In some cases, the He/H_2 permeation rates for the unglazed pellets were measured at elevated temperatures. The heater controller setpoint was increased in steps from 25°C to 330°C over several hours with measurements taken at each stable temperature operating point. The elevated temperature measurements were not made in all cases because the first several tests showed the He and H_2 permeation rates for the unglazed samples did not change significantly with increasing temperature (~30% reduction from 20°C to 330°C). Furthermore, the measured permeation rates for the unglazed pellets were generally >1000X greater than those of the glazed samples, so the contribution of the pellet permeation resistance was insignificant.

After measuring the permeation rates of the unglazed samples, the samples were coated with glaze (see Section 2.1) and then remeasured. The permeation rate measurements for the glazed samples were conducted similarly to the process used for the unglazed samples. Multiple temperatures were tested for each sample over the range of 25°C to 330°C. In addition, the source gas pressure was also varied to determine the relationship between gas pressure and the He/H_2 permeation rates.

The pressure-change tests showed the permeation rate of helium to be directly proportional to the helium pressure difference, as expected. For H_2, however, the tests showed a square-root-of-pressure dependence. This Sievert's-Law-type pressure effect was evidence that the H_2

permeation measurements were being driven by permeation of H_2 through the stainless-steel tubing in the test fixture rather than permeation through the $LiAlO_2$ pellet. This supposition was proved by a permeation test run using a test fixture with only the steel components (i.e., no $LiAlO_2$ pellet). The H_2 permeation rate for the pellet-less test fixture, shown in Figure 2.5 was found to be approximately equal that of the fixture with the glazed pellet.

Figure 2.5. Test fixtures with pellets removed to test for H_2 permeation through the steel

Because the tests with the pellet-less test fixtures showed the H_2 permeation through the steel components was overwhelming the pellet permeation measurement, the pellet test fixture was modified to remove the steel components. The stainless-steel tube portion of the fixture was replaced with two additional $LiAlO_2$ tubes bonded lengthwise as shown below in Figure 2.6. The three $LiAlO_2$ tubes form a single $LiAlO_2$ tube that is about 6 inches long. One end is plugged with either a SS441 plug coated with glass (to reduce its H_2 permeability) or a ceramic plug (both options were tested and yielded similar results).

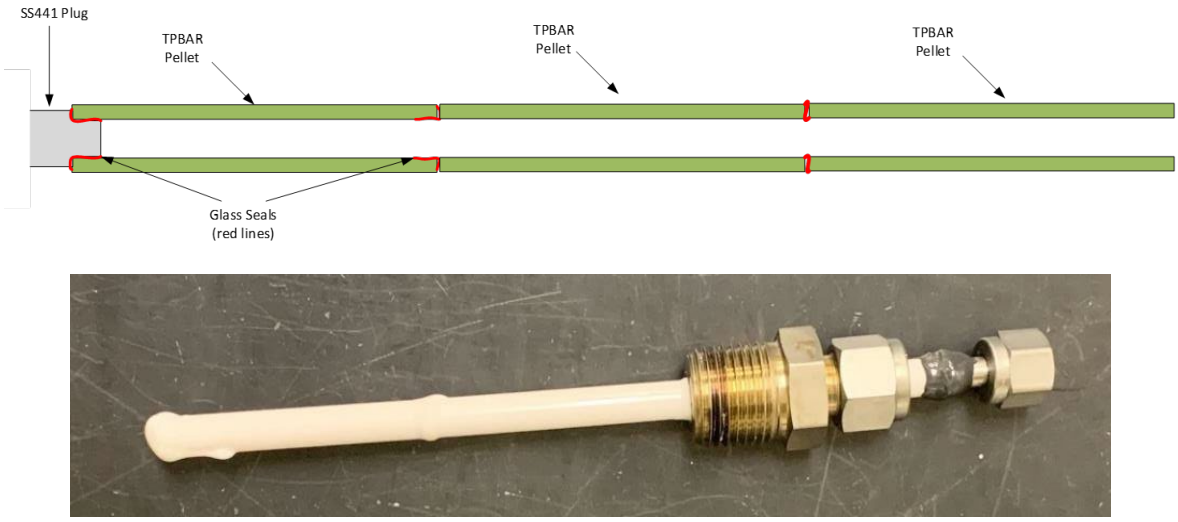

Figure 2.6. Test fixture made from three $LiAlO_2$ tubes bonded lengthwise

The open end of the 3-pellet $LiAlO_2$ tube was passed through a drilled-out Swagelok fitting and then sealed to the fitting using a Teflon ferrule under light compression. The open end of the tube was hermetically sealed to a steel fitting connected to the He/H_2 leak detector using J-B Weld epoxy. This test fixture was then used to make measurements of H_2 permeation rate for the samples. The helium/hydrogen leak detector can measure helium leak rates between 3E-12 and 1E-2 Torr-L/s, but the range for H_2 measurement is limited to about 4E-7 and 1E-2 Torr-L/s. The elevated lower limit for H_2 measurement is due to the desorption of H_2 from the stainless-steel components within the leak detector. Because of this limit, H_2 permeation measurements were successfully made only on the 3-pellet-stack sample with a 45-μm-thick glaze layer (i.e., sample #11). The thicker glaze layer of sample #14 yielded H_2 permeation rates too small to be reliably measured using the He/H_2 leak detector.

Permeation rates for water vapor were measured using a Pfeiffer OmniStar residual gas analyzer (RGA). The He/H_2 leak detector only monitors for helium and hydrogen, so an alternative instrument was needed to detect H_2O permeation. The RGA was used to sample the gas permeating through the pellet sample. First, the RGA setup was "calibrated" by measuring the helium permeation rate with the helium leak detector and then measuring the RGA signal intensity under identical pressure/temperature conditions. The helium was then evacuated from the 1-L test vessel and replaced with steam at 330°C and 64 psia. The resulting increase in the 18 amu signal intensity on the RGA was then used to estimate the H_2O permeation rate. The permeation rate is directly proportional to the RGA signal intensity after correcting for differences in the ionization sensitivities (I_s) of helium (I_s = 0.18) and H_2O (I_s = 1.12). There is a significant background signal at 18 amu in the RGA due to adsorbed water inside the vacuum chamber. Most mass-spectrometer systems suffer from this same limitation. Efforts were made to "bake out" the water as much as possible, but the remaining water signal was still relatively large compared with the signal resulting from H_2O permeation through the glaze. As a result, the H_2O permeation rate could only be measured for the thinnest glaze layer (~18 μm, samples #5 and #6).

3.0 Results and Discussion

3.1 CTE of As-Received $LiAlO_2$ Pellet

The thermal expansion behavior of an as-received sintered $LiAlO_2$ pellet was measured axially using a machined half pellet (1" long). The thermal expansion behavior of the substrate material is vital for selecting a good glaze candidate because residual stresses could be large enough to cause cracking in the glaze layer after firing if a large CTE mismatch exists between the substrate and the glaze. The thermal expansion behavior of the as-received $LiAlO_2$ pellet is shown in figure 3.1. The average CTE (from RT to 1000°C) was calculated to be ~12.6x10^{-6}/°C and ~12.4x10^{-6}/°C for two separate samples, showing consistent results. CTE of the candidate SCN-1 glaze material is ~10-11.0x10^{-6}/°C (Liu et al 2010). For samples to be operated at RT, the CTE mismatch between $LiAlO_2$ and the glaze may be considered undesirable. However, the very low glass transition (T_g) of SCN-1 glass (~500°C) can greatly reduce the residual stress since the residual stress is directly proportional to the temperature difference between T_g and the operation temperature (~330°C for $LiAlO_2$). In addition, the glaze will be under hoop compressive stresses while the $LiAlO_2$ pellet is under tensile stresses. The compressive stresses on the glaze would also minimize the cracking formation, hence SCN-1 was selected as a candidate glaze material where the chemical compatibility and irradiation stability remains to be evaluated.

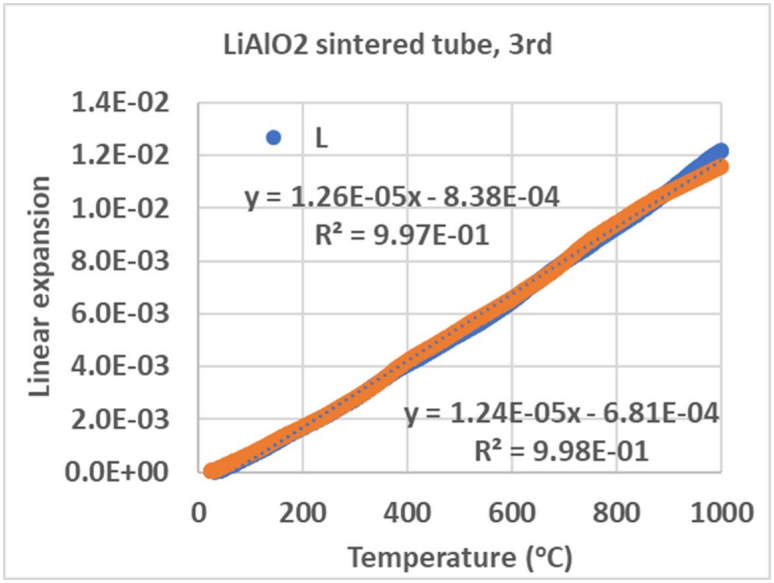

Figure 3.1 Linear thermal expansion behavior of as-received sintered $LiAlO_2$ pellet. Note two samples were tested and both showed similar linear behavior, implying no phase changes (a desirable characteristics for developing glaze material).

3.2 Wetting and Microstructure of Candidate Glaze Material

To achieve complete coverage of the glaze material on a sintered $LiAlO_2$ pellet, the wettability needs to be verified. To facilitate processing, we decided to use a surrogate material consisting of a ceramic bilayer with zirconia as outer layer, to mimic the oxide surface of $LiAlO_2$. The

ceramic coupons were dip coated with SCN-1 glaze slurry, dried, and fired at various temperatures (i.e., 750, 800, 850, and 900°C) for 2h. The coupons were then cross-sectioned and hand polished for optical microscopic examination of the contact angle. All samples showed a contact angle of less than 50 degrees, consistent with reported values (Lara-Curzio 2010), indicating good wetting of the SCN-1 glass on oxide surfaces. The appearance of SCN-1 glass dip-coated (2x) on ceramic bilayers after firing at various temperatures and times is shown in figure 3.2. It is evident that firing at 900°C for 2h resulted in the desired smooth surface and good coverage. At higher magnification, the rough morphology caused by trapped pores can be seen as shown in figure 3.3. The smoothest sample (900°C) has the lowest vol% of pores and the smallest pores. From a permeation perspective, a dense glaze with minimum porosity is preferred. The effect of the number of dip-coats (i.e., thickness) on the glaze microstructure was investigated for samples fired at 800°C for 2h with 1x to 4x dip-coats. Clearly, the porosity and pore sizes appear to increase with glaze thickness. At higher firing temperature (900°C/2h), the sample dip-coated 1x and 2x have the best microstructure with minimum porosity and pore sizes while the thicker coating (3x and 4x) exhibited pores that were larger in size and number. This likely arises from glaze viscosity, which increases with decreasing temperature, and glaze thickness increasing the time it takes for the pores to escape the glaze. At 900°C firing where the viscosity is lower, the pores can move more quickly up to surface and burst without coalescence, especially with 1x or 2x dip-coats where the distance to the surface is shorter. For thicker coats (3x and 4x), the pores do not have enough time to move up to surface and burst. For lower temperature (800°C), the viscosity may be high enough that very few pores escape the glaze.

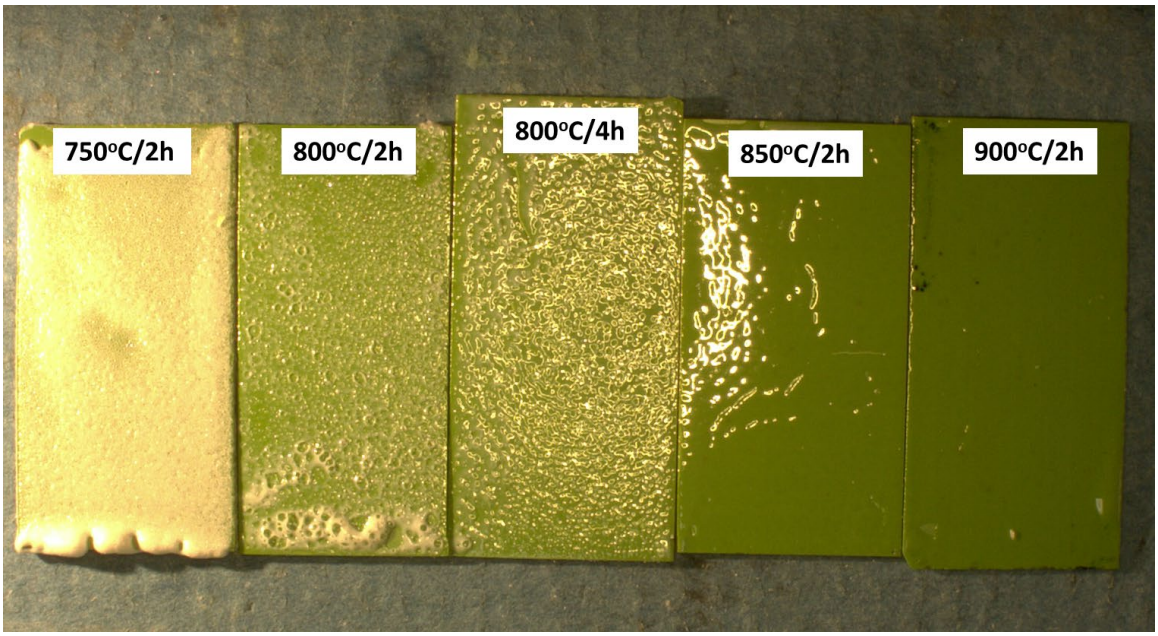

Figure 3.2 Appearance of SCN-1 glass dip-coated (x2) on bilayers after firing at different temperatures and times. The sample fired at 900°C showed the smoothest surface, indicating less bubbling.

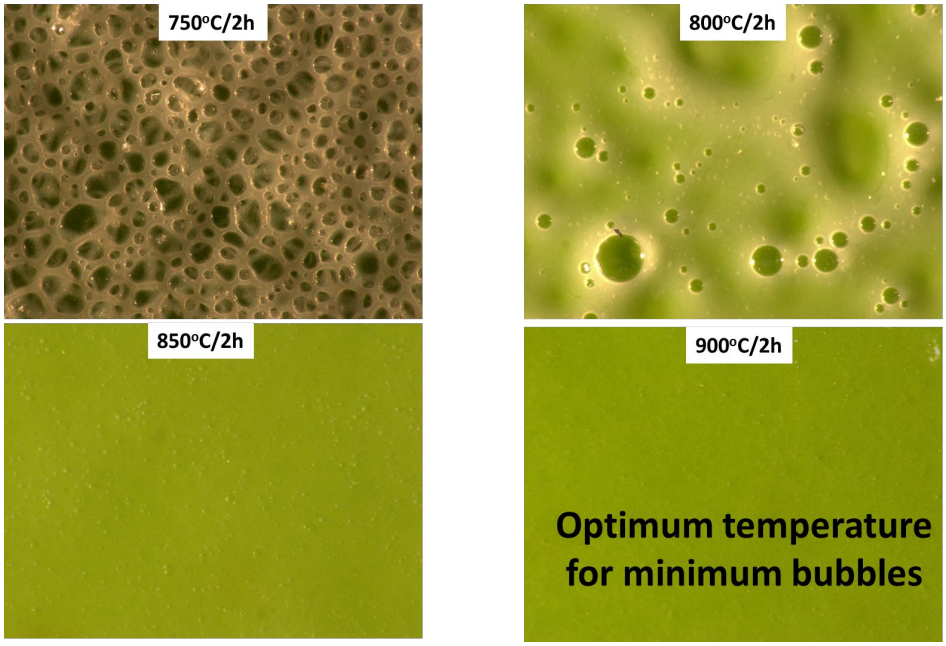

Figure 3.3 Appearance of SCN-1 dip-coated (2x) on ceramic bilayer after firing at various temperature for 2h in air, indicating 900°C firing is the optimum temperature with minimum pores.

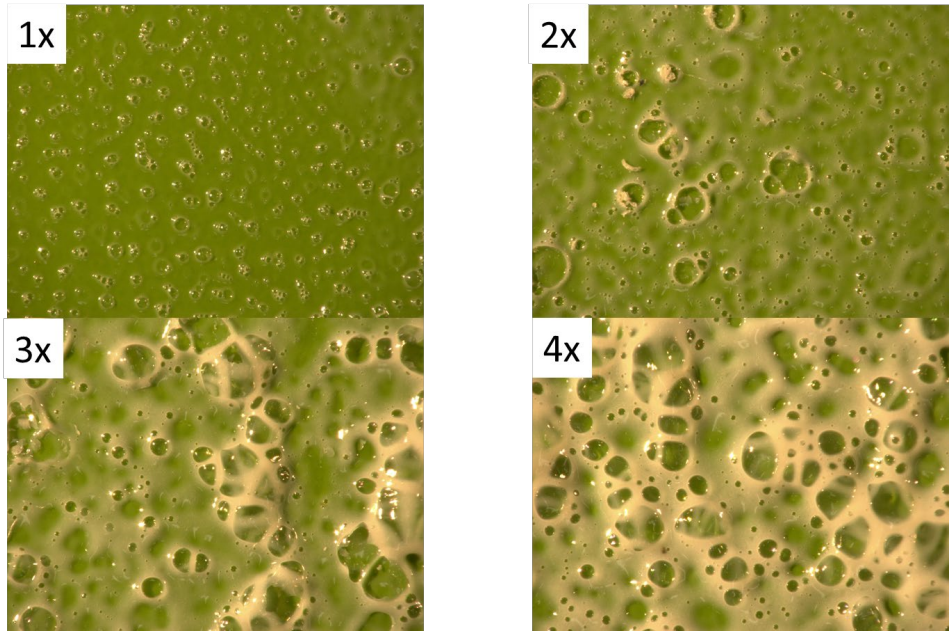

Figure 3.4 Appearance of SCN-1 dip-coated (1x to 4x) on ceramic bilayer after firing at 800°C for 2h in air, indicating pore size and volume increases with increasing number of dip-coats.

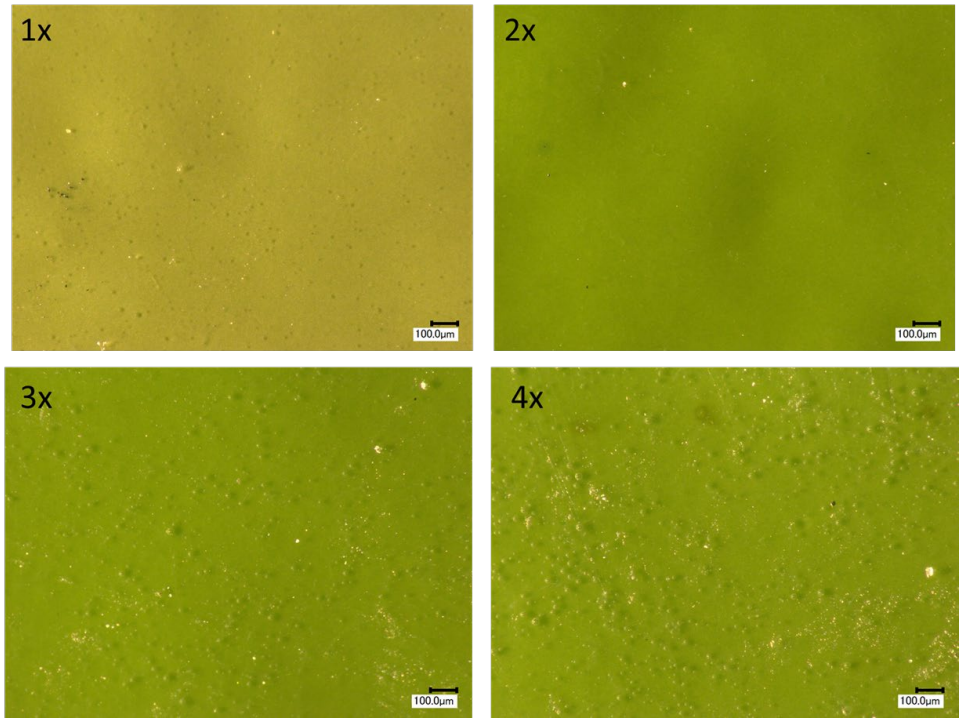

Figure 3.5 Appearance of SCN-1 dip-coated (1x to 4x) on ceramic bilayer after firing at 900°C for 2h in air, indicating that the thicker glaze resulted in more porosity and larger pores.

3.3 Effect of Number of Dip-Coats on Thickness

One important engineering aspect for glazing by dip coating is the empirical relationship between the number of dip-coats and fired glaze thickness. Above we determined that the best firing temperature for SCN-1 glass was 900°C, and the thickness study was therefore carried out at this temperature with 1x, 2x, 3x, and 4x coats with a fixed time of 2h. After firing, the sample was hand ground to reveal the cross-section, and glaze thickness was determined by OM on 10 different locations. A typical cross-sectional view is illustrated in figure 3.6. The results are shown in figure 3.7. Clearly, the glaze thickness increases linearly with the number of dip-coats. There may be some thickness variation along the longitudinal direction, especially at the bottom edge due to residual dripping from the 2" long pellet. This may be of no concern for actual pellets where the pellets are shorter.

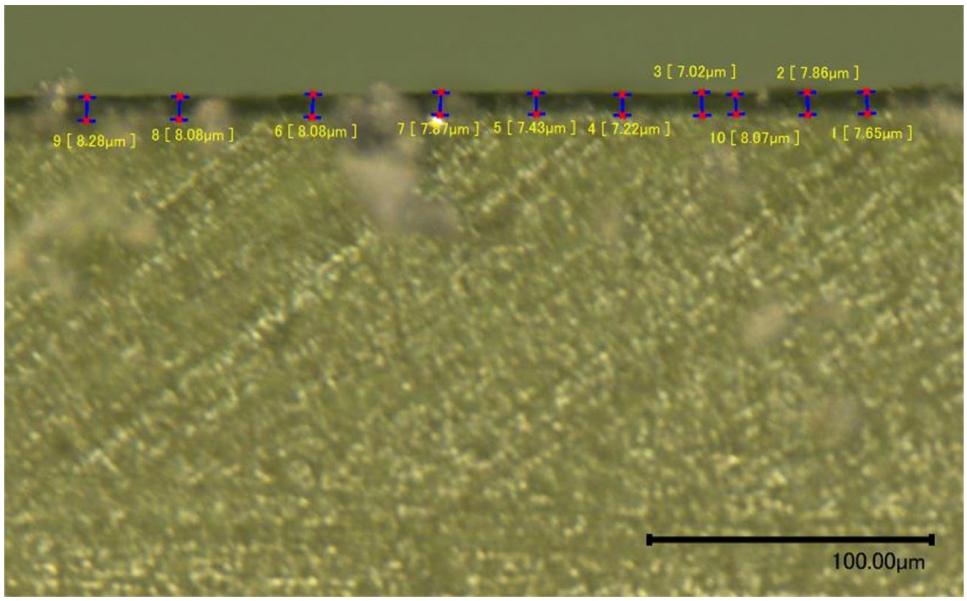

Figure 3.6 Typical cross-section of glazed (1x) sample after firing at 900°C 2h.

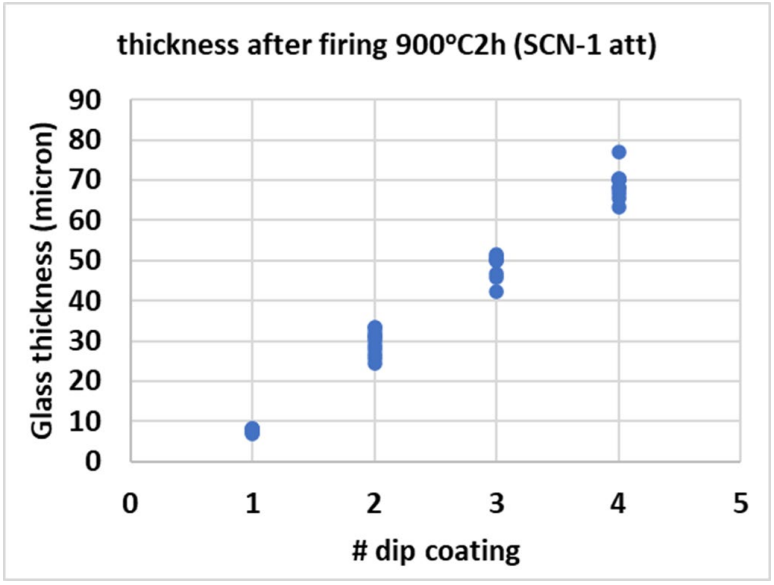

Figure 3.7 Effect of number of dip-coats on the glaze thickness after firing at 900°C 2h.

3.4 Chemical Compatibility

In addition to good wetting, matching CTE, and stability of the vitreous microstructure (no crystallization and grain boundary formation), the glaze on $LiAlO_2$ sintered ceramics should also be chemically compatible at sealing temperatures. The only concern would be the potential reaction of molten glass with $LiAlO_2$ at the sealing temperature of 900°C. A glazed (1x) pellet was sectioned and polished after firing for microstructural analysis along the glaze/$LiAlO_2$ interface. Figure 3.8 shows the typical interface microstructure by scanning electron microscopy (SEM) and the elemental analysis of Si, K, and Al was conducted by energy dispersive spectroscopy (EDS). From the SEM image, it's evident the glaze bonded well to the $LiAlO_2$ substrate without interfacial fracture or delamination occurring during the cutting and polishing processes. The surface of glaze also appeared relatively flat, consistent with previous characterization by optical microscopy. The thickness is around 4-5 microns, lower than the results from figure 3.7 (less than 10 microns). This may be due to the small field of view under SEM. The corresponding EDS analysis of Si. K, and Al showed no distinct reaction between SCN-1 and the $LiAlO_2$ pellet, indicating SCN-1 has good chemical compatibility.

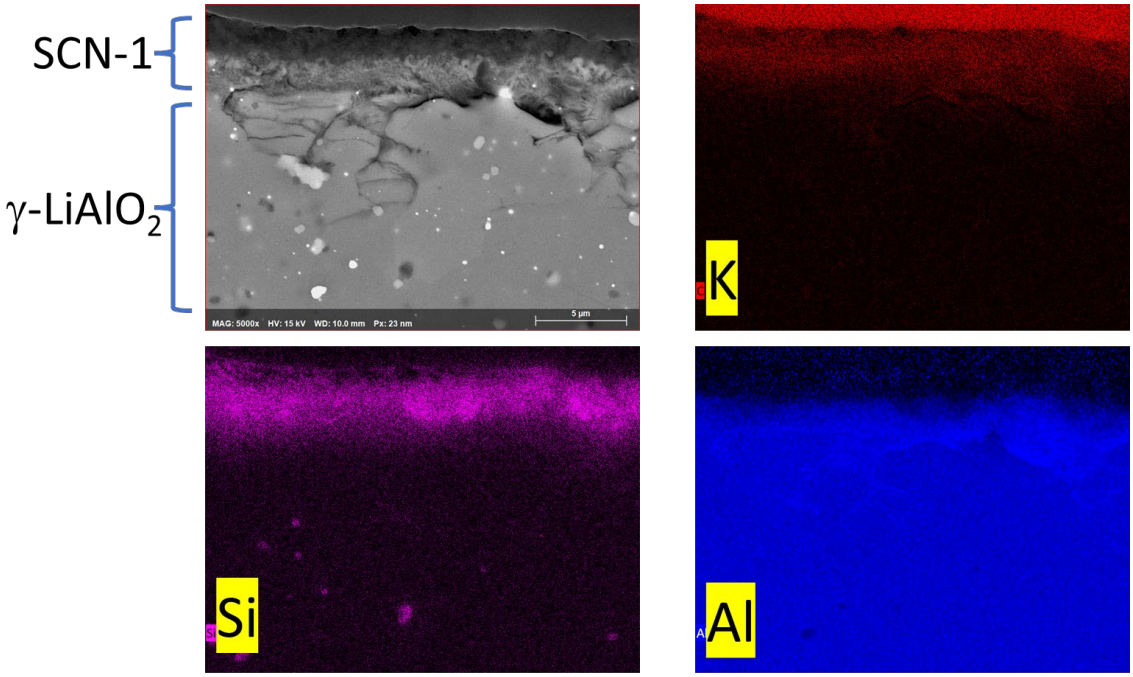

Figure 3.8 Microstructure of fired glaze pellet (900°C 2h) along the glaze/$LiAlO_2$ interface. The corresponding elemental analysis of Si, K, and Al is also shown.

3.5 Helium permeation measurements

Permeability (K) has units of mol/(s*Pa*m) is defined by the following equation:

$$K = \frac{qd}{A\Delta P}$$

where q = permeation rate (mol/s)
A = area of the pellet for permeation (m^2)
ΔP = pressure difference between the inside and outside of the pellet (Pa)
d = thickness of the pellet wall or glaze layer (m)

A numerical model of tritium release from TPBAR pellets was used to identify the target range of glaze permeabilities for the $LiAlO_2$ pellets. If the glaze permeability is too low, helium, T_2, and T_2O pressures will increase inside the pellets and eventually break open the glaze layer. If the glaze permeability is too high, then the helium/T_2/T_2O will be freely released, but the glaze will offer relatively little benefit in terms of reducing tritium permeation to the reactor coolant system.

The numerical model indicated that the target helium permeability should be in the range of about 1E-19 to 1E-17 mol/(s*Pa*m) at ~330°C for an assumed 100-micron-thick glaze layer. With this range in mind, we surveyed literature values for glass permeability to find suitable glaze candidates. A soda-lime glass (SCN-1) was identified as a good candidate based on its good thermal expansion match with $LiAlO_2$ and its reported permeability range. This is the glaze material that was used for all the work described in this report.

The permeation rates measured using the He/H_2 leak detector and the RGA were used along with estimates of the glaze layer thicknesses to calculate the glaze permeability for each sample exposed to each gas. This section summarizes the data collected and the permeability values calculated from the measured permeation rates. Sections 3.1, 3.2, and 3.3 describe the permeation results for helium, hydrogen, and water/steam, respectively. Section 3.4 includes numerical modeling of the predicted reduction in T_2 permeation rates for glazed pellets.

Helium permeation measurements were conducted as described in Section 2. The pellet-only helium permeation rates were measured before the samples were glazed and then remeasured at temperatures ranging from 20°C to 330°C. Permeation rates for two samples (#5 and #6) were measured after receiving one layer of glaze. Sample #11 was measured after application of 3 glaze layers and sample #14 was measured after 4 glaze layers. Additional samples were prepared but not yet tested.

Glaze layer thicknesses were estimated by the mass gain of the samples. There is likely significant variation in the glaze layer thickness over the surface of each pellet; future work could focus on better characterization of the glaze thickness uniformity. A small section of Sample #3 was prepared and examined by optical microscopy. This sample had three glaze layers applied. Visual examination of the glaze layer indicates a thickness of about 35 μm (see Figure 3.9). The weight-gain approach implies a layer thickness in the 40-50 μm range.

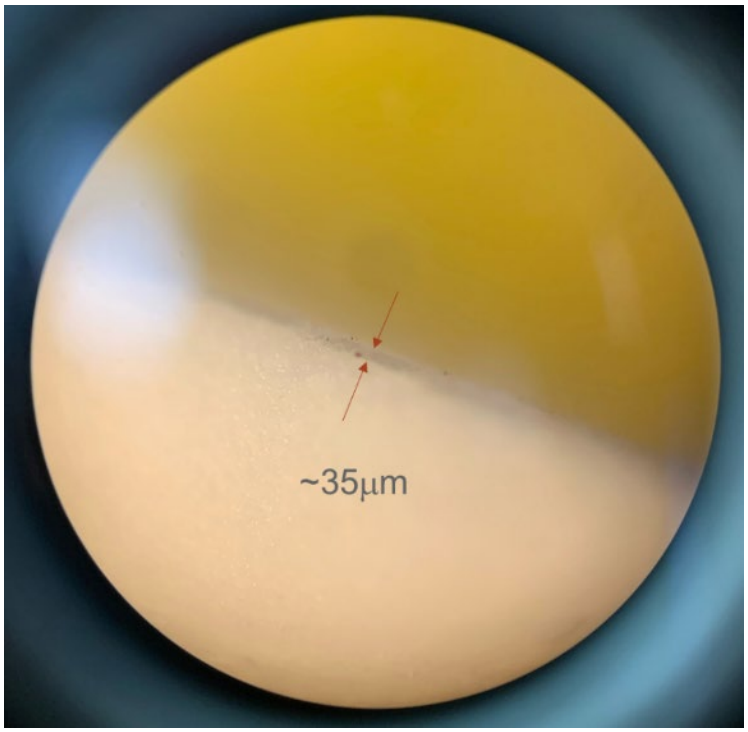

Figure 3.9. Glaze layer thickness for sample with 3 coats of glaze

The helium permeation test results are shown for samples #5 and #6 in Figures 3.X2 and 3.X3 below. Both tests were conducted using a 1-atm pressure differential across the $LiAlO_2$ pellet samples. At time = 9 hours for sample #6, the pressure differential was increased to 2.55 atm and the helium permeation rate increased in direct proportion from 1.8E-7 to 4.4E-7 Torr-L/s (2.44X). The “steady-state” permeation rate values were recorded for each stable temperature and used to calculate helium permeability values for the glaze layer. The calculated helium permeabilities for samples #5 and #6 are provided in Tables 3.1 and 3.2, respectively.

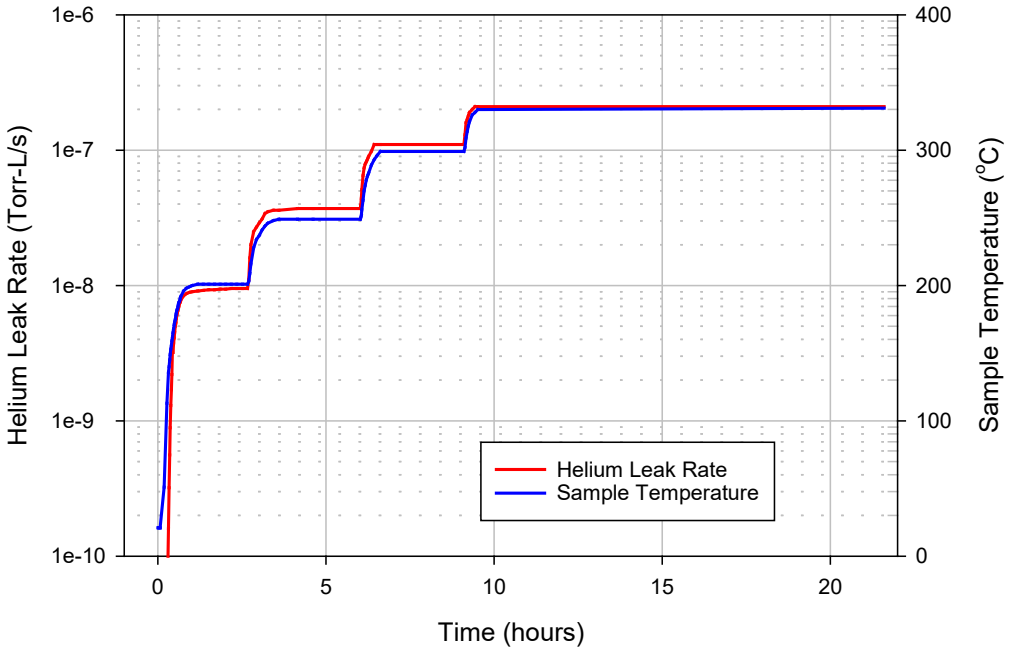

Figure 3.10. Measured Helium permeation rates for sample #5 vs. time and temperature

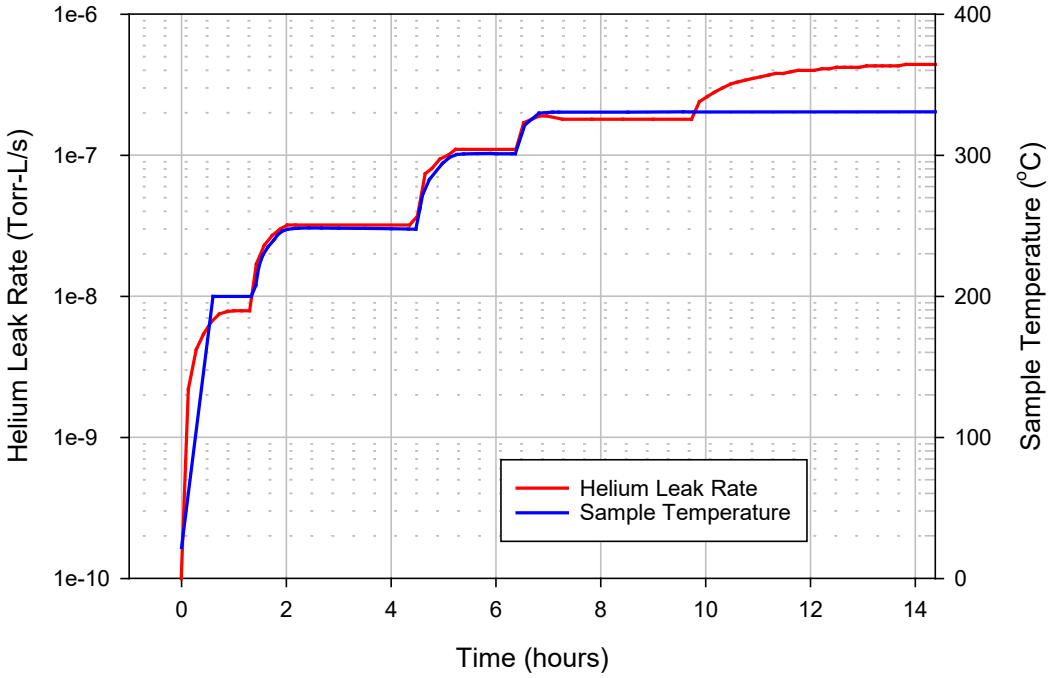

Figure 3.11. Measured Helium permeation rates for sample #6 vs. time and temperature

Table 3.1. Helium Permeation Data for Sample #5

Temp. (°C)	Glaze Thickness (μm)	Pellet-only helium Perm. Rate (Torr-L/s)	Glazed Pellet Helium Perm. Rate (Torr-L/s)	Pellet Permeability (mol/(s-Pa-m))	Glaze Permeability (mol/(s-Pa-m))
22	18	7.2E-4	4.2E-11	4E-13	4.0E-22
201	18	7.2E-4	9.5E-9	4E-13	8.9E-20
249	18	7.2E-4	3.7E-8	4E-13	3.5E-19
299	18	7.2E-4	1.1E-7	4E-13	1.0e-18
331	18	7.2E-4	2.1E-7	4E-13	2.0E-18

Table 3.2. Helium Permeation Data for Sample #6

Temp. (°C)	Glaze Thickness (μm)	Pellet-only helium Perm. Rate (Torr-L/s)	Glazed Pellet Helium Perm. Rate (Torr-L/s)	Pellet Permeability (mol/(s-Pa-m))	Glaze Permeability (mol/(s-Pa-m))
20	18	1.2E-4	5.8E-11	6E-14	5.5E-22
200	18	1.2E-4	7.9E-9	6E-14	7.4E-20
248	18	1.2E-4	3.2E-8	6E-14	3.0E-19
301	18	1.2E-4	1.1E-7	6E-14	1.0E-18
331	18	1.2E-4	1.8E-7	6E-14	1.7E-18

The helium permeability data for samples #5 and #6 are plotted versus inverse absolute temperature in Figure 3.12. The red line represents permeability data for soda-lime glass taken from Norton (1953). The permeabilities for the SCN-1 used for the present study are consistently about one-tenth those of the soda-lime glass reported by Norton, but the slope of the line is reassuringly similar. The difference between our data and that of Norton may be due to differences in glass composition as well as uncertainty in our effective glaze layer thicknesses.

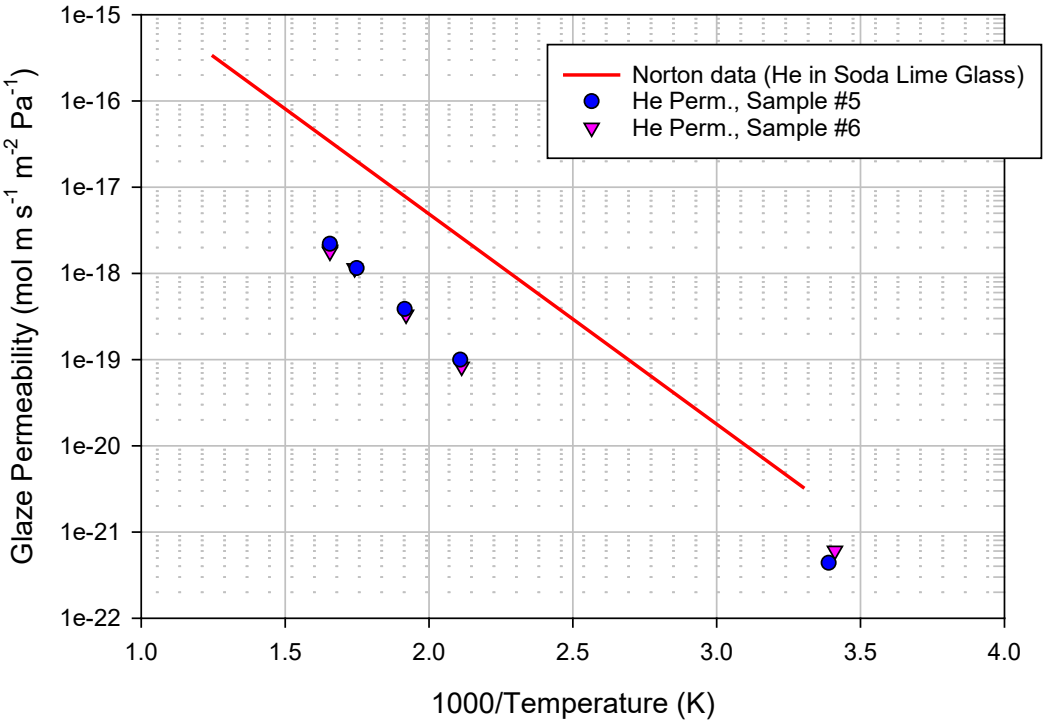

Figure 3.12. SN-1 glaze helium permeability measurements compared with literature curve

Helium permeation data were collected for samples with thicker glaze layers (#11 and #14) at 330°C and 1 atm pressure differential. The steady-state permeation rate values and calculated glaze permeability values are provided in Table 3.3 below.

Table 3.3. Helium Permeation Data for Samples #11 and #14 at 330°C

Sample	Glaze Thickness (μm)	Pellet-only helium Perm. Rate (Torr-L/s)	Glazed Pellet Helium Perm. Rate (Torr-L/s)	Pellet Permeability (mol/(s-Pa-m))	Glaze Permeability (mol/(s-Pa-m))
11	45	5.6E-4	7.2E-8	3E-13	1.7E-18
14	65	5.2E-4	1.6E-8	3E-13	5.4E-19

The helium permeation rates at 330°C for glazed samples 5, 6, 11, and 14 are plotted in Figure 3.13 versus estimated glaze-layer thickness. As expected, increasing the glaze thickness decreases the helium permeation rate. The permeation rate difference between the 18 μm sample and the 45 μm sample is as expected (i.e., inverse relationship with glaze thickness). This is evident in that the permeability values for these three samples (5, 6, and 11) are all approximately equal to 2E-18 mol/(s-Pa-m). The permeability for sample #14 (65 μm thickness) is only about 25% that of the other samples. The source of this discrepancy is not yet known.

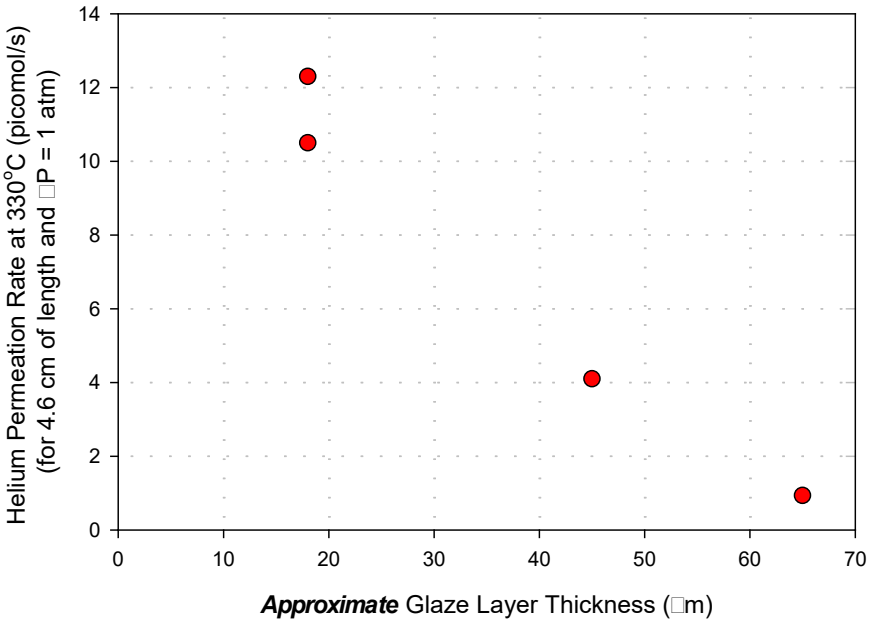

Figure 3.13. Effect of glaze thickness on helium permeation rate

Multiple tests of the unglazed pellets revealed that there is relatively little change in the helium and hydrogen permeation rates as temperature increases from 20°C to 330°C. An example test is shown in Figure 3.14. This test was conducted using a "three pellet stack" sample composed only of unglazed $LiAlO_2$ pellets and glass seals between the pellets. To ensure the measured permeation was exclusively through the pellet surfaces and not through the glass-seal joints or the end-plug, the seals and end-plug were covered with high-temperature epoxy. The test sample is shown in Figure 3.15. Previous tests had shown the epoxy has negligible helium or hydrogen permeability at temperatures below 250°C. The data in Figure 3.14 show relatively little change in the helium and hydrogen permeation rates over the range tested. Other tests using samples without epoxy coating showed a similar result for helium permeation up to 330°C. Based on these results, the unglazed pellet permeation rates were usually only measured at room temperature to characterize the very small contribution of pellet resistance to the measured glaze permeation rate.

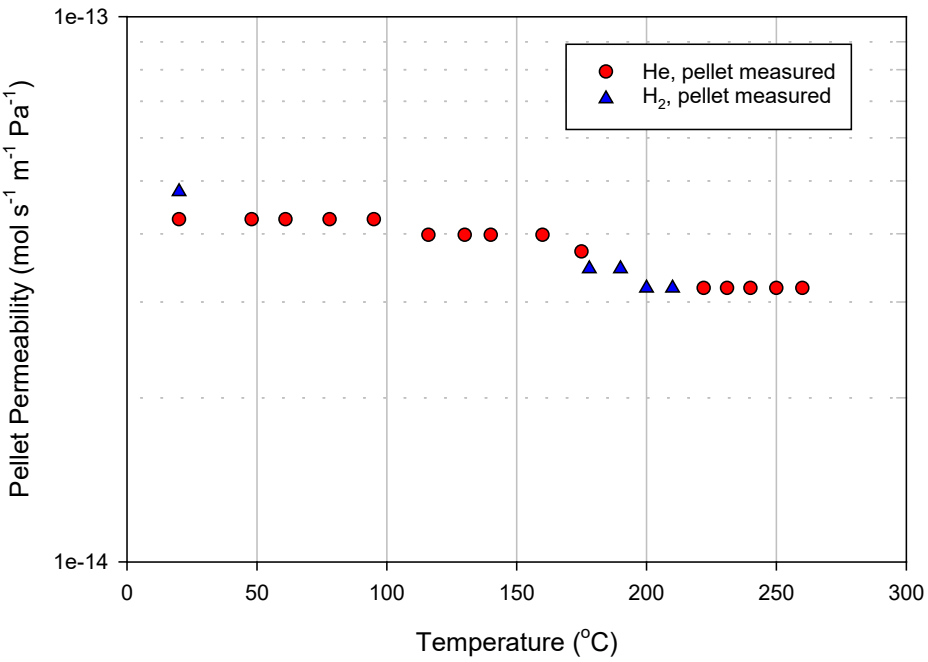

Figure 3.14. Effect of temperature on He/H_2 permeation rate in unglazed pellet

Figure 3.15. Unglazed 3-pellet test piece with epoxy covering joints and end-plug

3.6 Hydrogen permeation measurements

As discussed in Section 2, hydrogen permeation measurements were complicated by unwanted permeation of hydrogen through the stainless-steel portions of the sample test fixture and by the relatively high background H_2 concentrations that result in low sensitivity for the He/H_2 leak detector.

Hydrogen permeation rate measurements were attempted with samples #5 and #6, but the measured permeation rates were found to be due to permeation through the steel portions of the sample fixture. Figure 3.16 shows the H_2 permeation rates measured for these two samples at 330°C compared with a "steel only" fixture (see Figure 2.5). The data in Figure 3.16 show the permeation rate for the "steel only" fixture was essential equal to (actually slightly higher than) that of the sample with pellets.

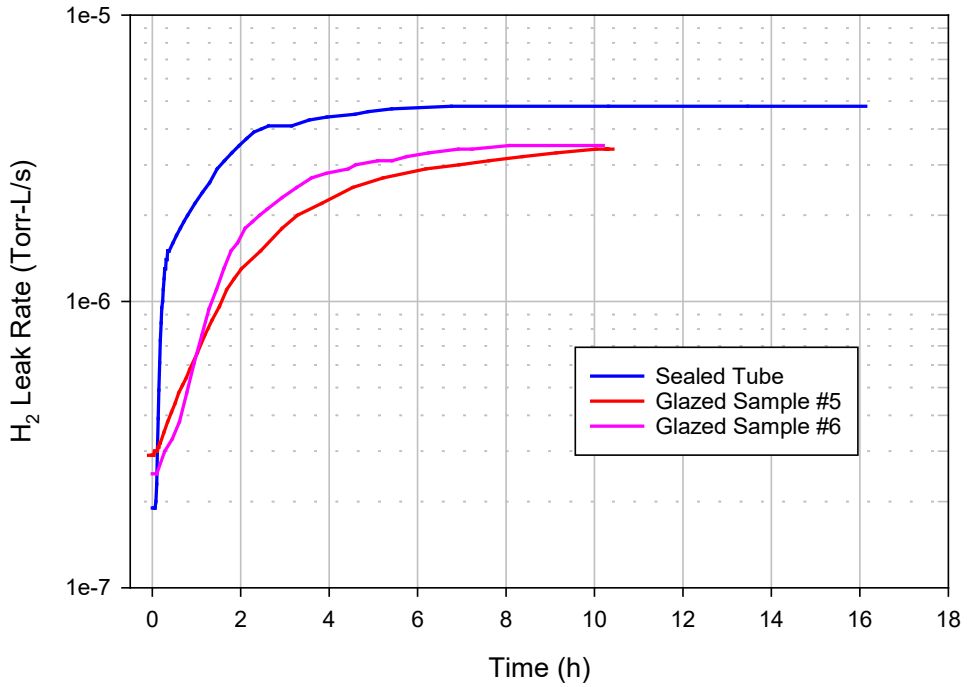

Figure 3.16. Hydrogen permeation rates at 330°C for samples 5, 6, and "steel only" fixture

The 3-pellet stack samples were developed after this problem was discovered. Samples #11 and #14 are 3-pellet stacks and hydrogen permeation rate measurements were made for both samples. The helium permeation rate for sample #11 was found to be 7.2E-8 Torr-L/s (corrected for permeation through a single pellet) for a differential pressure of 1 atm, which yields a helium permeability of 1.7E-18 mol/(s-m-Pa). The sample was then tested with H_2 using a 2.3 atm pressure differential and the H_2 permeation rate was measured at 1E-8 Torr-L/s. Correcting for the increased H_2 pressure results in a H_2 glaze permeability value of 1E-19 mol/(s-m-Pa), which is ~6% of the helium permeability.

An attempt was made to measure the H_2 permeation rate for sample #14, but the rate was found to be less than the detection limit for the He/H_2 leak detector. The permeation rate measured for sample #11 was just slightly greater than the detection limit.

Based on the sample #11 measurement, we expect the hydrogen permeation rate to be on the order of 6% that of the helium permeation rate. There is considerable uncertainty in this value; the uncertainty in the leak detector reading implies a range of 3% to 7%, but there are likely other error sources that could increase this range. However, other researchers have reported hydrogen permeation rates through glasses that are approximately 10% that of helium, so our result is reasonably consistent with the results of others (e.g., Leiby and Chen, 1960).

3.7 Water/steam permeation measurements

The He/H_2 leak detector does not measure water vapor leak rates, so an alternative approach was needed. To measure water permeation, a Pfeiffer OmniStar RGA was connected to the

fixture for Sample #5. The RGA and sample capillary were baked out for several days to reduce the water background at 18 amu.

The helium signal on the RGA was then measured to provide a calibration against a measurement made by the helium leak detector under the same conditions. The 330°C test vessel was pressurized with helium at 4.3 atm (absolute). The 4 amu signal (helium) stabilized at 4.9E-11 amps. The helium was then removed from the pressure vessel and replaced with 5.3 atm of steam. The 18 amu baseline increased by 2.2E-11 amps when the steam was added to the pressure vessel. The RGA data are plotted in Figure 3.17 below. The x-axis is time and covers approximately 24 hours of test time.

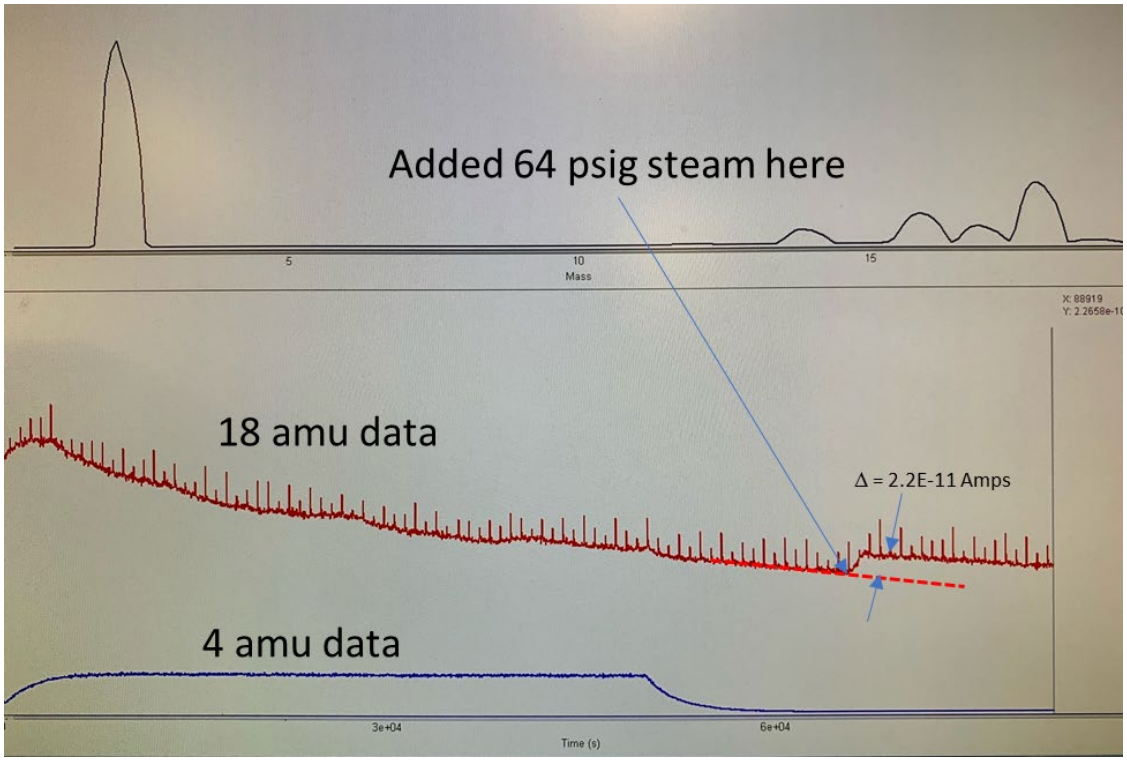

Figure 3.17. RGA data for water permeation measurement using Sample #5

Helium and water differ significantly in their ionization sensitivities. Higher ionization sensitivities will reflect proportionally larger signal levels from the RGA. The ionization sensitivity (I_s) of helium is 0.18 and that of water is 1.12. Adjusting the helium RGA current upward by a factor of 1.12/0.18 = 6.2X and then adjusting for the H_2O/helium pressure difference factor of 5.3/4.3 = 1.2X yields an adjusted helium RGA current of 3.8E-10 amps. The ratio of the observed 18 amu current (2.2E-11 amps) to the adjusted 4 amu current (3.8E-10 amps) is 0.06. Based on this measurement, the water permeation rate appears to be about 6% that of the helium permeation rate.

Attempts were made to perform this same measurement on Samples #11 and #14, but the signal levels were too low to be confident of the results.

3.8 COMSOL Modeling of Glaze Effect on Permeation of T_2

The goal of the present work is to evaluate the feasibility of using a thin glaze layer on the TPBAR pellets to reduce permeation of tritium to the reactor coolant system (RCS). The results described in the previous sections were focused on demonstrating the application of glaze to the pellets and characterizing the helium, hydrogen, and water-vapor permeation rates through the glaze. In this section, we describe predictions for the impact of the glaze layers on the rate of tritium permeation to the RCS.

For these analyses, the permeation rate of tritium is assumed to be approximately equal to that of hydrogen. Similarly, the T_2O permeation rate is assumed to be about equal to that of H_2O. These are reasonable assumptions; others have shown that isotope permeation rates tend to vary approximately via a square-root-of-mass-ratio relationship (e.g., Norton, 1953; Table VI). The permeation rates of T_2 and T_2O are, therefore, expected to be slightly lower than the corresponding rates for H_2 and H_2O.

The physics governing release of T_2 and T_2O from TPBAR pellets during in-reactor tritium production are not fully understood. For our analyses here, we are assuming that T_2O exists within the pellets in equilibrium with corresponding metal hydroxides (e.g., LiOT) as was discussed in Section 1.0. This assumption implies the T_2O will remain bound within the pellet as solid hydroxide except for a relatively low vapor pressure of T_2O expressed in equilibrium with the solid. An example solid/vapor equilibrium relationship between H_2O and LiOH is shown in Figure 3.18 below.

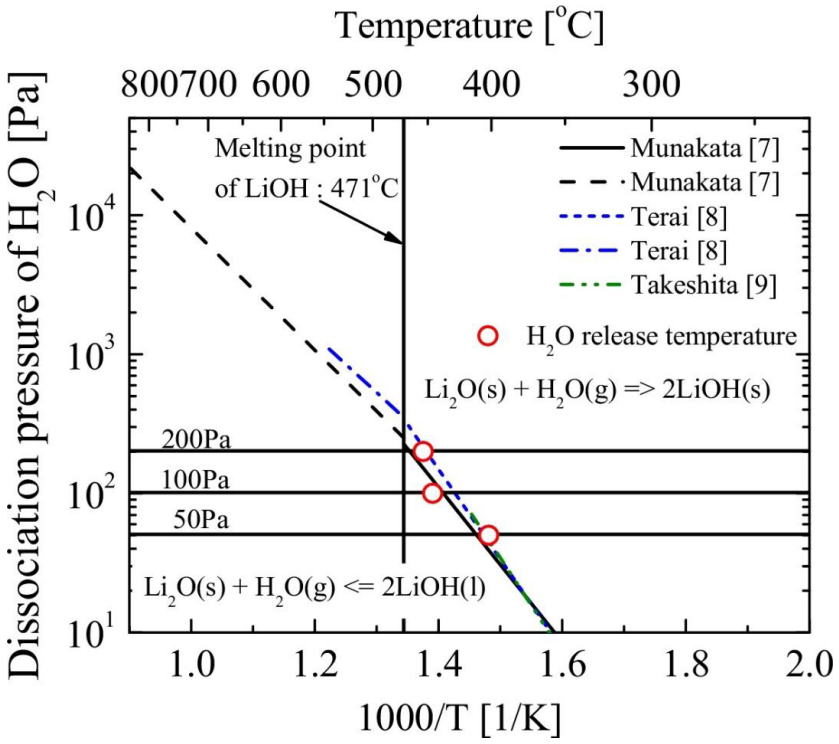

Figure 3.18. H_2O vapor equilibrium with Li_2O and LiOH from Katayama et al. (2016)

TPBAR pellets are heated to approximately 330°C during in-reactor tritium production; this corresponds to a 1000/T value of 1.65, which implies a $H_2O_{(g)}$ vapor pressure in equilibrium with LiOH in the range of about 10-20 Pa. For our tritium-release modeling described in this section, we are assuming the maximum partial pressure of T_2O that can be expressed within the pellets is ~20 Pa. As tritium is produced, some fraction is released promptly as T_2 and the rest remains bound within the pellet as LiOT according to the reaction:

$$5LiAlO_2 + 2n \rightarrow LiAl_5O_8 + 2LiOT + 2He$$

The tritium in the LiOT then gets released via diffusion/permeation through the pellet under its equilibrium vapor pressure of about 20 Pa.

A model for tritium release from TPBAR has been developed and is described in an internal document (i.e., TRIT-E-WP-007, Rev. 1 by Schmitt and Powell, 2023). The baseline assumption in this model is that tritium is produced as primarily T_2 early in the cycle with progressively more T_2O being produced later. The baseline production rates are plotted over the assumed 500-day cycle in Figure 3.19 below.

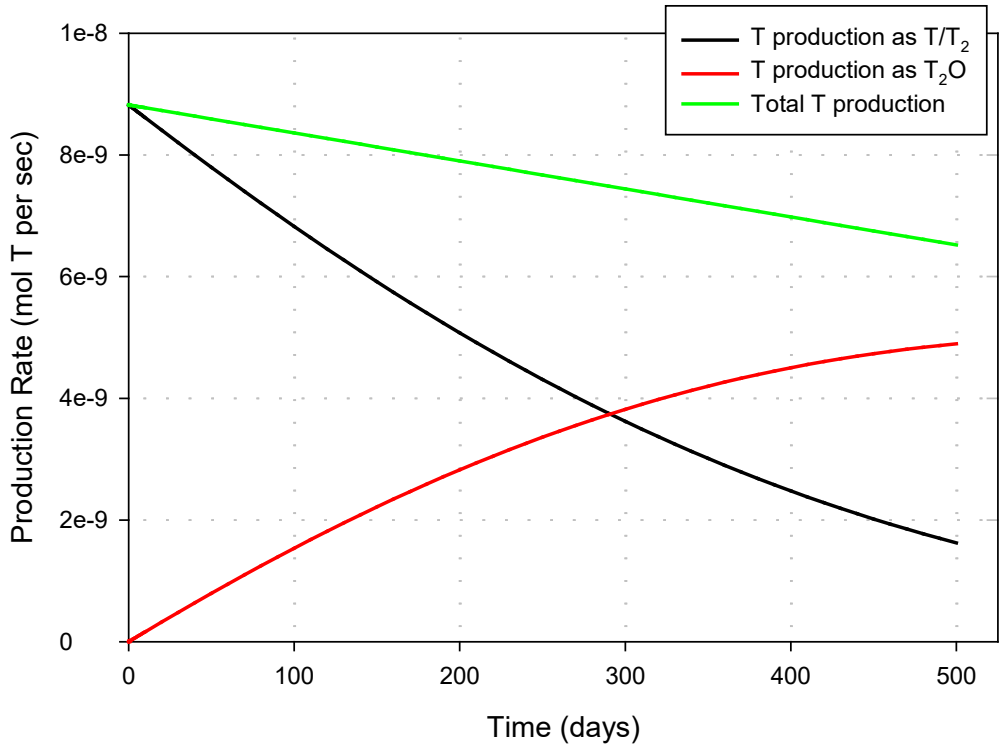

Figure 3.19. Baseline T_2 and T_2O release rates from TPBAR pellets as assumed in COMSOL model

The split between T_2 and T_2O production rates shown in Figure 3.19 is an *assumption* that has not, as far as we are aware, been supported experimentally. Alternative T_2/T_2O production splits might be more representative. With this in mind, we evaluated a variety of different assumptions when simulating tritium release to the RCS by glazed and unglazed pellets.

For the glazed-pellet simulations, the entire external surface of the pellets was assumed to be coated in SN-1 glaze to a thickness of 18 μm (identical to samples #5 and #6 described in this report). The helium glaze permeability was taken to be 2E-18 mol/(s-m-Pa) and the T_2 and T_2O permeabilities were both set to 6% of that value to be consistent with our measurements.

Figure 3.20 shows the COMSOL modeling results for predicted tritium permeation to the RCS under a variety of assumed T_2/T_2O split ratios. The black line shows the "no glaze" baseline prediction, which uses the T_2/T_2O production split shown in Figure 3.19. The green line shows the effect of adding the glaze layer to the pellets under the baseline T_2/T_2O split assumption. In this case, the glaze is predicted to have only a small effect on tritium permeation. The reason for this small effect is that the high levels of T_2 production early in the cycle force the getter to reach its "plateau" region wherein the T_2 pressure expressed on the outside of the getter does not significantly change as more T_2 is absorbed. Since the glaze primarily restricts T_2O release (under the assumptions described above), the total permeation of tritium to the RCS is relatively unaffected by the glaze.

However, if more of the tritium is produced as T_2O in the pellet rather than as T_2 then the glaze shows a much more significant beneficial effect. The other lines plotted in Figure 3.20 show assumptions of 90% T_2O, 99% T_2O, and 99.9% T_2O, all of which are expected to result in significant reductions in tritium release to the RCS.

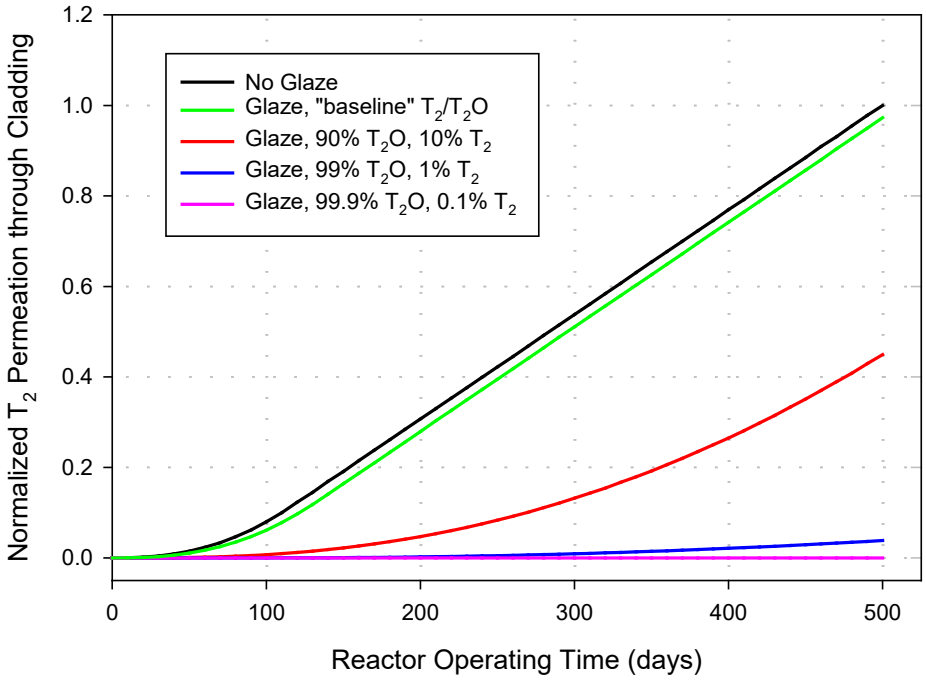

Figure 3.20. Predicted tritium release to the RCS; effect of glaze and assumed T_2/T_2O split

Based on the modeling results shown above, whether the glaze layer offers a beneficial effect depends strongly on the nature of the tritium release from the pellets. If the primary release of tritium is via vapor pressure of T_2O expressed in equilibrium with LiOT then we expect a significant reduction in tritium permeation to the RCS because the glaze layer will effectively restrict release of T_2O from the pellet while allowing release of helium and, to a lesser extent, T_2.

Without additional information regarding T_2/T_2O production and release in TPBAR pellets the accuracy of our predictions for a beneficial effect of glaze on the pellets is unknown. It is currently unclear how to improve these predictions, but the results of planned/ongoing experiments might help resolve the issue (e.g., TMIST-3 and TMIST-4).

However, as part of our work we noticed something unexpected and interesting. As described earlier, the first step in our pellet/glaze characterization tests involves measuring the permeation rate of the unglazed pellets. These measurements were made on dozens of unglazed pellets. Figure 3.21 compares H_2 diffusivity values for permeation through unglazed pellets with the pellet diffusivity used in the TPBAR COMSOL model. The measurements made as part of this work imply H_2 diffusivities more than 5 orders of magnitude greater than the value used in the COMSOL model.

It is unclear whether the value used in the COMSOL model is based on measurements for H_2 diffusion through $LiAlO_2$ ceramic or if it is just a value that was selected to yield about the right amount of T_2/T_2O retention in the pellet at end of cycle. Typically, around 40% of the produced tritium remains inside the pellet at the end of the 500-day cycle with the rest being bound in the zirconium getter. Using a T_2 diffusivity of about 3E-15 m^2/s for diffusion through the pellet allows the model to predict about the right amount of tritium (as T_2 and T_2O) remaining in the pellet at end of cycle.

However, if the model is adjusted to use a diffusivity value consistent with our permeation rate measurements (~1E-9 m^2/s), *then the pellet is predicted to effectively contain zero tritium* (T_2 + T_2O) at end of cycle. Based on this discrepancy, it seems the T_2/T_2O production assumption reflected in Figure 3.19 is, at a minimum, incomplete.

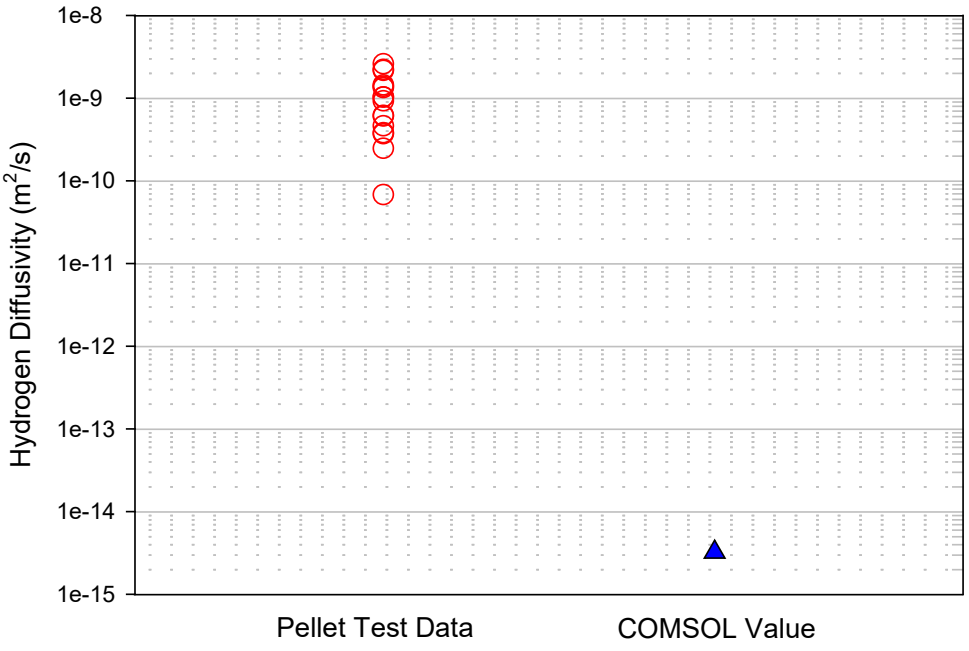

Figure 3.21. H_2 diffusivity values based on unglazed permeation rates compared with COMSOL model value

The H_2 diffusivities for the unglazed pellet were measured primarily at 20°C, but several pellets were tested over the full 20°C to 300°C range and relatively little variation was found. Figure

3.22 shows data for one of the pellet tests (He and H_2 diffusivities) compared with the COMSOL model diffusivity for H_2. This discrepancy in diffusivities is not attributable to differences in temperature.

One possible explanation for this discrepancy is that the T_2 and T_2O effective diffusivities[1] in the pellets really *are* on the order of 1E-9 m^2/s and the rate of T_2/T_2O release from the pellets is governed by a pressure-limiting effect such as the T_2O/LiOT equilibrium. To illustrate this point, we made two changes to the COMSOL TPBAR model. First, we changed the diffusivities for T_2 and T_2O to match the values measured in the present work (i.e., ~1E-9 m^2/s for T_2). Second, we adjusted the tritium production assumption such that all tritium is produced as T_2O in equilibrium with LiOT. Along with this second change, we incorporated the assumption that the T_2O vapor pressure is maintained at a maximum 20 Pa.

With these changes to the model, the predicted total tritium remaining in the pellet at the end of cycle is approximately 50%, which is consistent with actual TPBAR pellet behavior. This agreement is obviously not proof that our assumptions are correct, but it does show that they lead to a prediction consistent with experience.

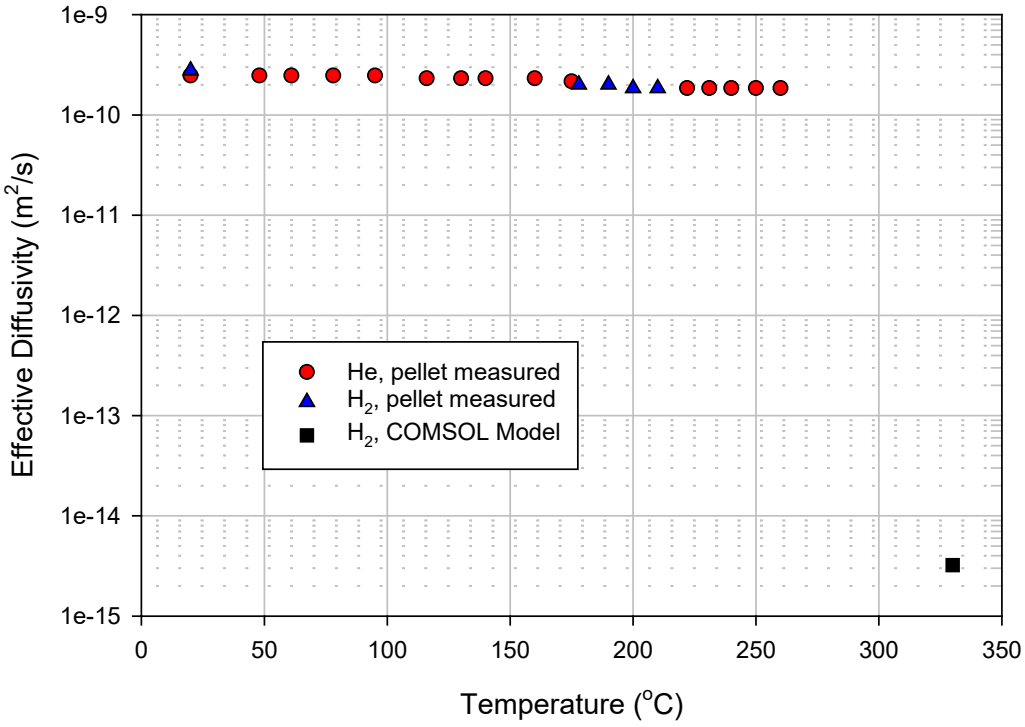

Figure 3.22. He and H_2 diffusivities for an unglazed pellet vs. temperature compared with the H_2 diffusivity used for the COMSOL model

[1] One possible interpretation of our observation is that we are measuring the gas permeation rate due to diffusion/flow along grain boundaries. The low diffusivity (~4E-15 m^2/s) used in the COMSOL model may apply to diffusion through $LiAlO_2$ *crystals*, but not include this grain-boundary effect that applies to the bulk of the pellet. Because the $LiAlO_2$ grains are relatively small (~2.5 µm, see Jiang et al., 2017), T_2 and T_2O should be able to rapidly diffuse out of the grains to reach the grain boundaries and then rapidly diffuse out of the pellet; the characteristic diffusion time under this scenario is only about 5 minutes, which is negligible relative to the timescales applicable to tritium production in the TPBAR (500-day cycle).

4.0 Conclusions

The work described in this report demonstrated successful identification and application of a candidate glaze material that is compatible with LiAlO2 pellets and has the targeted gas-permeation properties. Demonstration of an appropriate glaze was the primary goal of this work. The key findings from this effort are as follows:

- Coating the $LiAlO_2$ pellets with SCN-1 glass appears to be feasible in that the molten glass readily wets the pellets and the thermal expansion match is good.
- The permeability of the SCN-1 glaze to H_2, H_2O, and He is in the targeted range and the required glaze thickness for the desired gas restriction would be approximately 20 μm, which represents only a small loss of TPBAR volume.
- The predicted effect of glazed pellets on tritium permeation to the reactor coolant system is uncertain due to current uncertainties in the nature of tritium release from the pellets. If a large fraction of the release is in the form of T_2O, for example, then a significant reduction in tritium permeation to the reactor coolant system is expected with the use of glazed pellets.
- The higher-than-expected permeability of unglazed pellets implies the assumed tritium release model used in the TPBAR COMSOL model is currently incomplete. As more is learned about the form of tritium production/release in the pellets, the model can be improved and used to make more reliable predictions for the effects of adding glaze layers to the pellets.

5.0 References

https://prod.cloudfront.making.unsw.edu.au/documents/GlazeTechnologyLearningResources.pdf, “Intro to Glaze Technology”.

Rosa Trejo, Edgar Lara-Curzio,*,†Amit Shyam,* Melanie J. Kirkham,Valerie Garcia-Negron, and Yanli Wang, “Physical and Mechanical Properties of Barium AlkaliSilicate Glasses for SOFC Sealing Applications,” International Journal of Applied Glass Science 3 [4] 369–379, 2012.

W.N Liu X. Sun E.V. Stephens M.A. Khaleel, “Investigation of Performance of SCN-1 Pure Glass as Sealant Used in SOFC”, PNNL Report 19407, March 2010.

Y-S Chou, E. C. Thomsen, J-P Choi, J. W. Stevenson, “Compliant alkali silicate sealing glass for solid oxide fuel cell applications: Combined stability in isothermal ageing and thermal cycling with YSZ coated ferritic stainless steels,” J. Power Sources, **197** 154-160, 2012.

Francis J. Norton, “Helium Diffusion Through Glass”, J. Am. Ceram. Soc., 37, 3, 37-109, 1953.

Jiang, W, J Zhang, DJ Edwards, NR Overman, Z Zhu L Price, J Gigax, E Castanon, L Shao, and DJ Senor. 2017. “Nanostructural evolution and behavior of H and Li in ion-implanted γ-LiAlO2.” J. Nucl. Matls. **494**:411-421.

Katayama, et al. 2016. “Pebble structure change of Li_2TiO_3 with excess Li in water vapor atmosphere at elevated temperatures.” *Nuclear Materials and Energy.* **9**:242-246

Leiby and Chen. 1960. “Diffusion Coefficients, Solubilities, and Permeabilities for He, Ne, H_2, and N_2 in Vycor Glass.” *J. Applied Physics.* **31**(2):268-274

Norton, FJ. 1953. “Helium Diffusion Through Glass.” *JACS*. 36(3):90-96

Wakabayashi and Tomozawa. 1989. “Diffusion of Water into Silica Glass at Low Temperature” *J. Am. Ceram. Soc.* **72**(10):1850-55

Pacific Northwest National Laboratory

902 Battelle Boulevard
P.O. Box 999
Richland, WA 99354

1-888-375-PNNL (7665)

www.pnnl.gov